

Modeling the behavior of hot oxygen ions

M. D. Zettergren¹, W. L. Oliver¹, P.-L. Blelly², and D. Alcaydé³

¹Boston University, Massachusetts, USA

²LPCE-CNRS, Orléans, France

³CESR-CNRS-UPS, Toulouse, France

Received: 16 November 2005 – Revised: 24 March 2006 – Accepted: 13 April 2006 – Published: 3 July 2006

Abstract. Photochemical processes in the upper atmosphere are known to create significant amounts of energetic oxygen atoms or “hot O”. In this research we simulate the effects of ionized hot oxygen, hot O⁺, on the ionosphere. We find that hot O⁺ is not able to maintain a temperature substantially above the ambient ion temperature at most altitudes, the exception being around the F-region ion density peak. However, the thermalization of hot O⁺, due to Coulomb collisions, represents an important heating process for the ambient ions. A time-dependent, fluid-kinetic model of the ionosphere (TRANSCAR) is used to self-consistently simulate hot O⁺ by considering it to be a separate species from O⁺. A Maxwellian neutral hot O population having characteristics consistent with current knowledge is added to TRANSCAR. The production of the hot O⁺ is then computed by considering ion charge exchange with the neutral hot O population that we have assumed. Loss of hot O⁺ results from these charge exchange reactions and from reactions with molecular atoms.

Keywords. Ionosphere (Ion chemistry and composition; Ionosphere-atmosphere interactions; Mid-latitude ionosphere)

1 Introduction

It has been observed that the ion temperature in the ionosphere significantly exceeds what theoretical calculations say the temperature should be, (Oliver and Glotfelty, 1996; Oliver and Schoendorf, 1999). A neglected heat source could account for this difference. This fact led researchers to propose the existence of a non-thermal population of oxygen atoms, known as hot O. There is considerable *in situ* evidence for the existence of hot O (Hedin, 1989; Cotton et al., 1993).

Correspondence to: M. Zettergren
(mattz@bu.edu)

While there are alternative explanations to Hedin’s conclusion of a population of hot O (Keating et al., 1997), there is also radar and optical evidence to support the existence of hot O. Oliver (1997) analyzed radar data and concluded that an unknown heat source for the ions, such as hot O, is needed to explain the observed ion temperature. Optical observations made by Hernandez (1971) show a broadened oxygen spectrum, indicating the presence a high-temperature population of oxygen. Most work estimates the effective temperature of hot O to be in the range of 4000 K–6000 K, and the concentration to be about 0.1%–1% of the cold O density at 400 km altitude, (Rohrbaugh and Nisbet, 1973; Shematovich et al., 1994; Oliver, 1997; Litvin and Oliver, 2000). The profile shape of the hot O density has not been determined conclusively; hot O could form a layer shape (Cotton et al., 1993; Schoendorf et al., 2000), it could approximate diffusive equilibrium (Oliver, 1997), or it could form some other type of exponential shape (Yee et al., 1980; Shematovich et al., 1994). Research has shown that hot O can be produced in numerous reactions (Richards et al., 1994; Hickey et al., 1995) and can have a potentially large effect on the energy dynamics of the ionosphere (Oliver, 1997; Alcaydé et al., 2001). Hot O ionizes in the same ways as thermal oxygen: via photoionization and charge exchange chemistry. Airglow observations have confirmed the fact that hot O⁺ can exist at least long enough to undergo radiative decay and emission (Yee et al., 1980). However, the production, loss, and heating effects of hot O⁺ have not yet been investigated in any detail, despite this evidence that supports its existence.

The purpose of our work is to make a first attempt to characterize hot O⁺ behavior and its effects on the upper atmosphere. We want to establish two main things. First, can hot O⁺ exist in appreciable densities? Second, can hot O⁺ maintain an elevated temperature significantly above the ambient ion temperature, or does it cool to the same temperature? We approach this goal in two ways. First we present a simplified analysis of the density and temperature of hot O⁺. Then

Table 1. TRANSCAR chemistry model for hot O^+ and the associated reactions rates. k_1 and k'_1 are taken from Stancil et al. (1999); k_3 and k_4 are taken from Diloy et al. (1996). We have assumed that $k_2=k_1$ since there are no available reaction rates for O^+ -O charge exchange.

(R ₁)	$H^+ + O_{\text{hot}} \xrightarrow{k_1} O_{\text{hot}}^+ + H$	$k_1=1.29 \times 10^{-9} e^{-227/T} (T/10000)^{0.517}$ $+4.25 \times 10^{-10} (T/10000)^{6.69 \times 10^{-3}}$
(R' ₁)	$O_{\text{hot}}^+ + H \xrightarrow{k'_1} H^+ + O_{\text{hot}}$	$k'_1=2.08 \times 10^{-9} (T/10000)^{0.405}$ $+1.11 \times 10^{-11} (T/10000)^{-0.458}$
(R ₂)	$O^+ + O_{\text{hot}} \xrightarrow{k_2} O_{\text{hot}}^+ + O$	$k_2=k_1$
(R' ₂)	$O_{\text{hot}}^+ + O \xrightarrow{k'_2} O_{\text{hot}} + O^+$	$k'_2=k'_1$
(R' ₃)	$O_{\text{hot}}^+ + O_2 \xrightarrow{k_3} O_2^+ + O$	$k_3=2.82 \times 10^{-11} - 7.74 \times 10^{-12} (T/300)$ $+1.073 \times 10^{-12} (T/300)^2$ $-5.17 \times 10^{-14} (T/300)^3$ $+9.65 \times 10^{-16} (T/300)^4$ (300 ≤ T ≤ 6000)
(R' ₄)	$O_{\text{hot}}^+ + N_2 \xrightarrow{k_4} NO^+ + O$	$k_4=1.533 \times 10^{-12} - 5.92 \times 10^{-13} (T/300)$ $+8.6 \times 10^{-14} (T/300)^2$ (300 ≤ T ≤ 1700) $=2.73 \times 10^{-12} - 1.155 \times 10^{-12} (T/300)$ $+1.483 \times 10^{-13} (T/300)^2$ (1700 ≤ T ≤ 6000)

we present a numerical simulation in which we integrate a hypothesized hot O population into the ionospheric model TRANSCAR (Blelly et al., 1996b; Diloy et al., 1996; Blelly et al., 1996a), and self-consistently model a hot O^+ population produced from the hot O.

2 Approximation of hot O^+ profile shape

We propose that, in the steady-state, hot O^+ forms a layer dominated by chemistry at lower altitudes and by diffusion at higher altitudes. A layer of this type has maximum density where the chemical loss time constant equals the diffusion time constant (Rishbeth and Garriot, 1969). The chemical reactions that we consider for hot O^+ are shown in Table 1. The loss processes for hot O^+ are the “primed” reactions, R1'–R4'. The chemical loss time constant for these reactions, β^{-1} , is given by:

$$[\beta(z)]^{-1} = \left[\sum_{i=1}^4 k'_i n_{N'_i}(z) \right]^{-1} \quad (1)$$

k'_i is the reaction constant for reaction R'_i, and $n_{N'_i}(z)$ is the number density of the neutral reactant of reaction R'_i as a function of altitude z . The diffusion time constant is given by Rishbeth and Garriot (1969):

$$\frac{H_s^2}{D(z)} = \frac{\left(\frac{k_b T_s}{m_s g} \right)^2}{m_s v_{sj}(z)} \quad (2)$$

Here $D(z)$ is the diffusion coefficient, H_s is the scale height for $s=O_{\text{hot}}^+$, k_b is Boltzmann’s constant, T_s is the temperature for species $s=O_{\text{hot}}^+$, v_{sj} is the collision frequency between species s and species j , m_s is the mass of species s , and g is the acceleration of gravity. The collision frequency that we are concerned with in this approximation is that of the dominant collision process involving hot O^+ , collisions with O^+ . With these considerations the hot O^+ layer density peak occurs where the chemical and diffusion time constants are equal.

$$\sum_{i=1}^4 k'_i n_{N'_i}(z) = \frac{k_b T_s}{m_s v_{sj}(z)} \quad (3)$$

For computation we adopt profiles for neutral densities and collision frequencies from our TRANSCAR control simulation. In this control simulation we use TRANSCAR to simulate the ionosphere without hot O or hot O^+ included. Using $T_s=4000$ K the peak of the layer occurs at $z_{pk} \approx 840$ km.

It is assumed that there is zero flux divergence at the hot O^+ density peak, and we consider only chemical sources on hot O^+ . Under these assumptions the density is given by the ratio of the production rate of hot O^+ to the loss frequency of hot O^+ , evaluated at the peak altitude z_{pk} .

$$\frac{q(z_{pk})}{\beta(z_{pk})} = \frac{[k_1 n_{H^+}(z_{pk}) + k_2 n_{O^+}(z_{pk})] n_{O_{\text{hot}}}(z_{pk})}{\sum_{i=1}^4 k'_i n_{N'_i}(z_{pk})} \quad (4)$$

k_1 is the reaction constant for reaction R₁ of Table 1, and k_2 is the reaction constant for reaction R₂. Our simulations

of hot O^+ show that the assumption of zero flux divergence at the peak is accurate and that photoionization can also be ignored. Again using values from the control simulation of TRANSCAR for the O^+ density and assuming hot O to be in diffusive equilibrium with a reference density of 1% of O density at 400 km, we find the hot O^+ peak density to be $n_s(z_{pk}) \approx 5.62 \times 10^{10} \text{ m}^{-3}$. Below this peak the hot O^+ density drops off with altitude as a result of increasingly rapid loss chemistry. Far above the hot O^+ peak, collisions, and thus chemical reactions, become scarce and diffusion dominates.

3 Approximation of hot O^+ temperature behavior

To analyze the behavior of the hot O^+ temperature, we first consider the case where a sample population of hot O^+ is injected into the ionosphere and allowed to “relax” and thermalize down to the temperature of the ambient ions.

The 1-D equation describing the evolution of the hot O^+ temperature with time is given by Blelly et al. (1996b):

$$k_b \frac{\partial T_s}{\partial t} + u_s k_b \frac{\partial T_s}{\partial z} + \frac{2}{3n_s} \frac{1}{A} \frac{\partial A q_s}{\partial z} = k_b \frac{\delta T_s}{\delta t} + \frac{2}{3n_s} (L_s - Q_s) \quad (5)$$

$$\frac{\delta T_s}{\delta t} = \frac{2}{3} \sum_j \frac{m_s v_{sj}}{m_s + m_j} \left[3 (T_j - T_s) + \frac{m_j}{k_b} (u_j - u_s)^2 \right] + \left(\frac{\delta T_s}{\delta t} \right)^* \quad (6)$$

For the case of the hot O^+ temperature $s=O^+$, z is the independent spatial variable (distance along magnetic field line), t is the independent time variable, and A is the cross section area of the magnetic flux tube as a function of z . L_s and Q_s are energy loss and source rates, respectively. $(\delta T_s/\delta t)^*$ is a source term, explained later, that includes energy input due to production processes. For our simplified calculations we assume that $Q_s=L_s=0$ and $(\delta T_s/\delta t)^*=0$.

We make a few approximations in order to solve Eq. (5). All drift velocities and the hot O^+ heat flow are assumed to be zero so that transport of energy becomes unimportant. This enables us to consider the temperature at a given altitude to be independent of the temperature at other altitudes, and to approximate how the hot O^+ temperature behaves as a function of time. With these approximations and noting that $s=O^+$, the temperature equation becomes:

$$\frac{\partial T_s}{\partial t} = -\frac{2}{3} \sum_j \frac{16v_{sj}}{16+m_j} 3 (T_s - T_j) \quad (7)$$

There is an equation of this form for the temperature at each altitude. Since Coulomb collisions dominate the dynamics of the F-region, the summation can be reduced to a sum over

the major ions, $j_1=O^+$ at lower altitudes and $j_2=H^+$ at high altitudes:

$$\frac{\partial T_s}{\partial t} = - \left(v_{sj_1} + \frac{32}{17} v_{sj_2} \right) T_s + v_{sj_1} T_{j_1} + \frac{32}{17} v_{sj_2} T_{j_2} \quad (8)$$

If the collision frequencies and temperatures vary slowly with time as compared to the hot O^+ temperature, then the solution of this equation is:

$$T_s(t) = C_1 + (T_s(t_0) - C_1) e^{-\nu'(t-t_0)} \quad (9)$$

$$\nu' = v_{sj_1} + \frac{32}{17} v_{sj_2} \quad (10)$$

$$C_1 = \frac{1}{\nu'} \left(v_{sj_1} T_{j_1} + \frac{32}{17} v_{sj_2} T_{j_2} \right) \quad (11)$$

From the solution for T_s it can be seen that $T_s(\infty)=C_1$. For most altitudes the O^+ and H^+ temperatures will be almost the same so the approximation $T_{j_1}=T_{j_2}=T_i$ is appropriate. Inserting these values for C_1 yields:

$$T_s(\infty) = T_i \quad (12)$$

This leads us to predict that hot O^+ thermalizes to the ambient ion temperature, T_i with an approximate time constant of $1/\nu'$, as seen from the solution for T_s . Using our control simulation to get representative values for the collision frequencies involved in these calculations, we obtain a value for the decay time constant $\tau=1/\nu'$ as a function of height. A plot of this time constant is shown in Fig. 1 along with a plot of the time constant found from our simulation of hot O^+ , which is discussed in detail later. As expected the time constant increases with altitude as collisions become increasingly infrequent.

The energy source, $(\delta T_s/\delta t)^*$, needs to be considered for determining the steady-state equilibrium temperature of hot O^+ . $(\delta T_s/\delta t)^*$ represents the energy released into the hot O^+ medium during its production, given by:

$$\left(\frac{\delta T_s}{\delta t} \right)^* = \frac{P_s (T_{O_{hot}} - T_s)}{n_s} \quad (13)$$

Here P_s represents the total production rate per unit volume of hot O^+ . Intuitively, $(\delta T_s/\delta t)^*$ is the rate of temperature change due to production of $s=O^+$. The main reactions that produce hot O^+ are charge exchange reactions involving neutral hot O, in which neutral hot O loses an electron to become hot O^+ . At the instant of creation, a hot O^+ ion has kinetic energy similar to that of the neutral hot O atom from which it is produced. The fluid description of ions that is used by TRANSCAR does not track individual particle energy, but, rather the average energy and temperature of each ion species population. Any hot O^+ produced by charge exchange is assumed to have the temperature of the rest of the population at the time of creation. To model the fact that the newly created hot O^+ has energy comparable to that of its

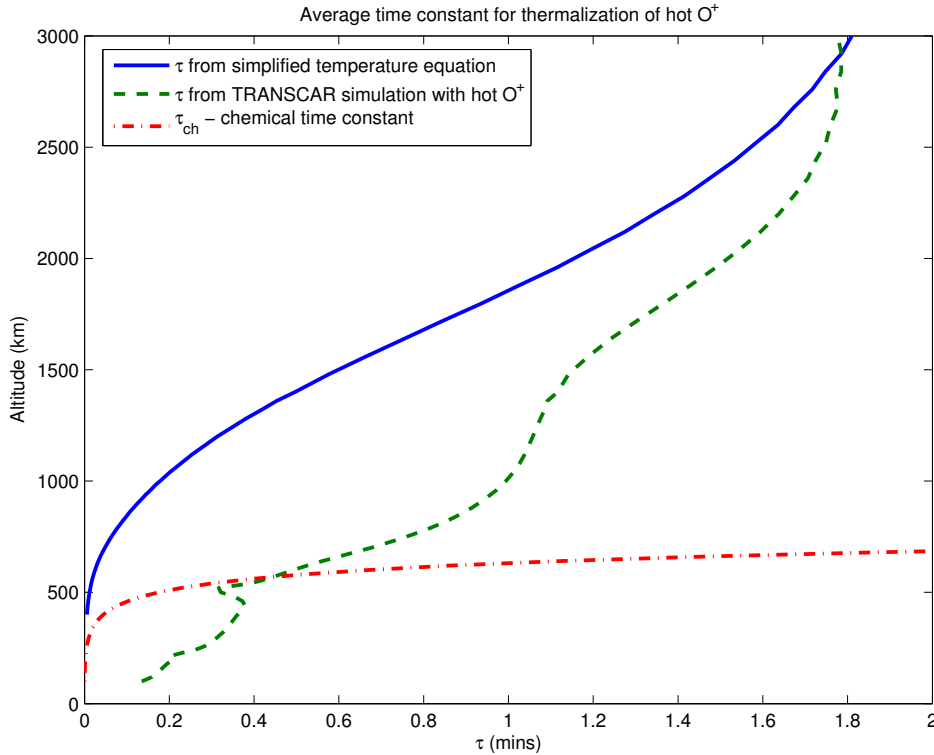


Fig. 1. Comparison of calculated and simulated thermalization time constants for hot O⁺. The chemical time constant (Eq. 1) is also shown for comparison.

parent, hot O atom and not the same energy as the “old” hot O⁺, the energy source of Eq. (13) is needed.

The expression for $(\delta T_s/\delta t)^*$ is derived by considering the energy exchange between neutral hot O and hot O⁺ during production processes involving these species. $(\delta T_s/\delta t)^*$ can be expressed in the following form:

$$\left(\frac{\delta T_s}{\delta t}\right)^* = \frac{2}{3k_b n_s} \left(\frac{\delta E_s}{\delta t}\right)^* - \frac{T_s}{n_s} \left(\frac{\delta n_s}{\delta t}\right)^* \quad (14)$$

$(\delta n_s/\delta t)^*$, the density change due to production, is P_s . By definition:

$$\left(\frac{\delta E_s}{\delta t}\right)^* = \int_{-\infty}^{\infty} \frac{\delta \varepsilon}{\delta t} d^3 c_s \quad (15)$$

$\delta \varepsilon/\delta t$ is the rate of energy released into the hot O⁺ medium due to production and c_s is the random velocity of the gas. If we assume that all energy is released at the same level $3/2 k_b T_{O_{hot}}$, then this expression becomes:

$$\begin{aligned} \left(\frac{\delta E_s}{\delta t}\right)^* &= \frac{3}{2} k_b T_{O_{hot}} \int_{-\infty}^{\infty} \left(\frac{\delta f_s}{\delta t}\right)^* d^3 c_s \\ &= \frac{3}{2} k_b T_{O_{hot}} P_s. \end{aligned} \quad (16)$$

This expression assumes that a newly created hot O⁺ ion inherits the kinetic energy of its parent atom. Substituting this

value for $(\delta E_s/\delta t)^*$ into Eq. (14) yields Eq. (13). The inclusion of a heat source due to chemical creation, $(\delta T_s/\delta t)^*$, can be applied to ions other than hot O⁺, as well. However, as seen from Eq. (13), this source term is significant only when the ion and its parent have a large temperature difference.

If the $(\delta T_s/\delta t)^*$ heat source is included, then the temperature equation can be solved for the steady state equilibrium temperature by setting $\partial T_s/\partial t=0$:

$$T_{s,eq} = \frac{\nu_{sj1} T_{j1} + \frac{32}{17} \nu_{sj2} T_{j2} + \frac{P_s}{n_s} T_{O_{hot}}}{\nu_{sj1} + \frac{32}{17} \nu_{sj2} + \frac{P_s}{n_s}} \quad (17)$$

$T_{s,eq}$ is now a weighted sum of the ion and hot O temperatures. In regimes where the production of hot O⁺ is large relative to its density, the equilibrium temperature is higher than T_i . However, at altitudes where the production is relatively low, this heat source can be ignored and the temperature of hot O⁺ is equal to that of the other ions. Our simulations will answer the question of at what altitudes P_s/n_s is large and the temperature of hot O⁺ remains elevated, and at what altitudes this heating effect is insignificant and the hot O⁺ thermalizes. It should also be noted that if Eq. (5) is solved with the $(\delta T_s/\delta t)^*$ term from Eq. (13) included, then the solution retains the form of Eq. (9) with $T_s(\infty)=C_1=T_{s,eq}$.

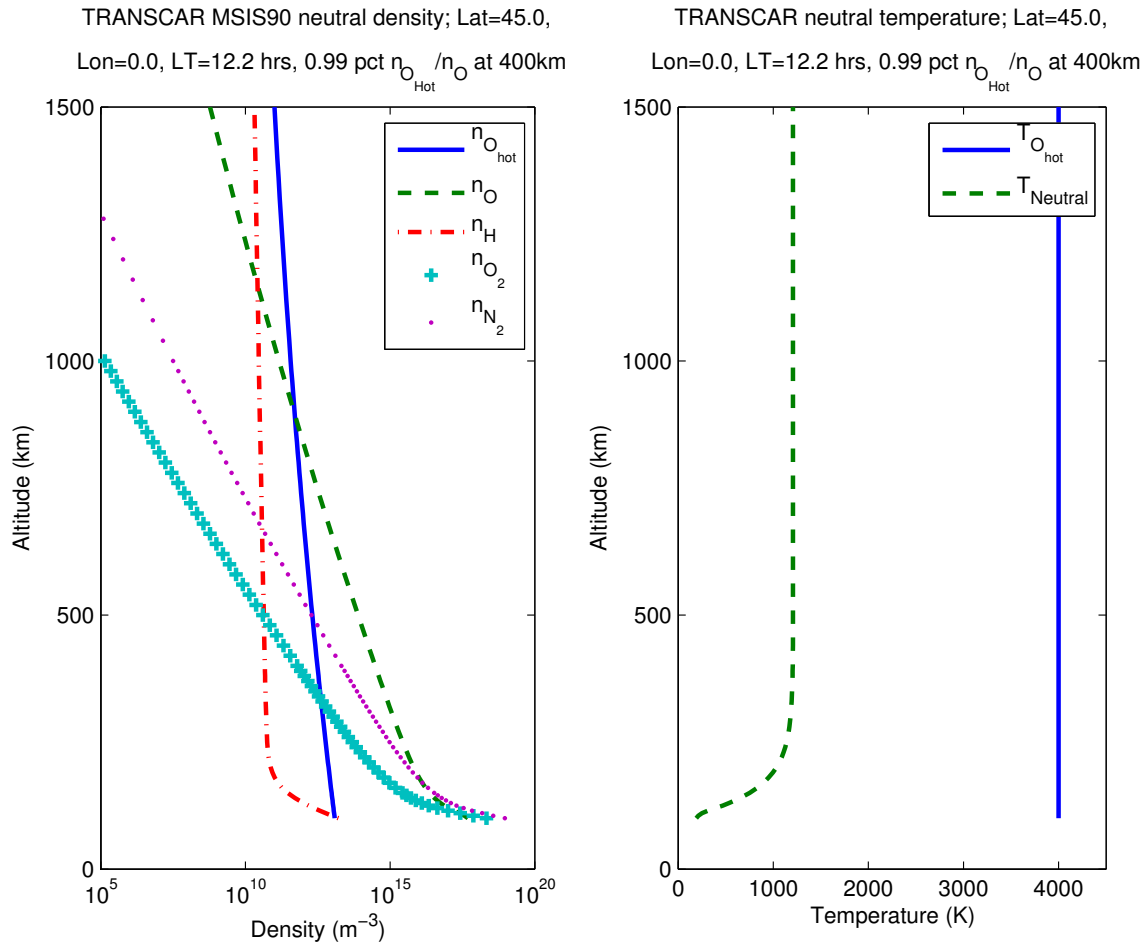


Fig. 2. The neutral atmosphere from TRANSAR. n_s is the number density for species s . $T_{O_{hot}}$ is the hot O temperature and $T_{Neutral}$ is the other neutral particle temperatures from the MSIS model.

4 Numerical modeling

The computer simulation that we use to model the effects of hot O on the ionosphere and the behavior of hot O^+ is TRANSAR (described in Brelly et al., 1996b). TRANSAR is a time-dependent, 8-moment fluid model of the ionosphere that solves for the density n_s , drift velocity u_s , temperature T_s , and heat flow q_s for 6 different ion species ($s=O^+, H^+, N^+, N_2^+, NO^+, \text{ and } O_2^+$). TRANSAR computes a numerical solution to the conservation equations for each of these moments in 1-D, along the geomagnetic field lines.

TRANSAR assumes the distribution function of the gases that it models to be adequately described with 8 moments. An 8-moment distribution function can describe gases that are somewhat non-Maxwellian through the heat flow vector, but a gas that is highly non-Maxwellian, such as a mixture of hot and cold oxygen, cannot be adequately accounted for in a 8-moment model. In the case of oxygen, the distribution function has a Maxwellian center that represents thermal, or cold O, with a pronounced high-energy tail that represents hot O. We have chosen to break apart the oxygen distribution function into ambient oxygen and hot O and model them as separate species with different distribution functions.

In this paper, we perform 3 simulations with TRANSAR. One simulation is a control and does not include hot O or hot O^+ . The second simulation includes just neutral hot O. The third includes both hot O and hot O^+ . All simulations are done during the month of October, for a latitude of 45° , $f_{10.7}=187$, and $K_p=0$.

5 Simulation with neutral hot O

We adopt a diffusive equilibrium density profile for the neutral hot O.

$$n(z) = n(z_0)e^{\frac{-(z-z_0)}{H(z)}}, \tag{18}$$

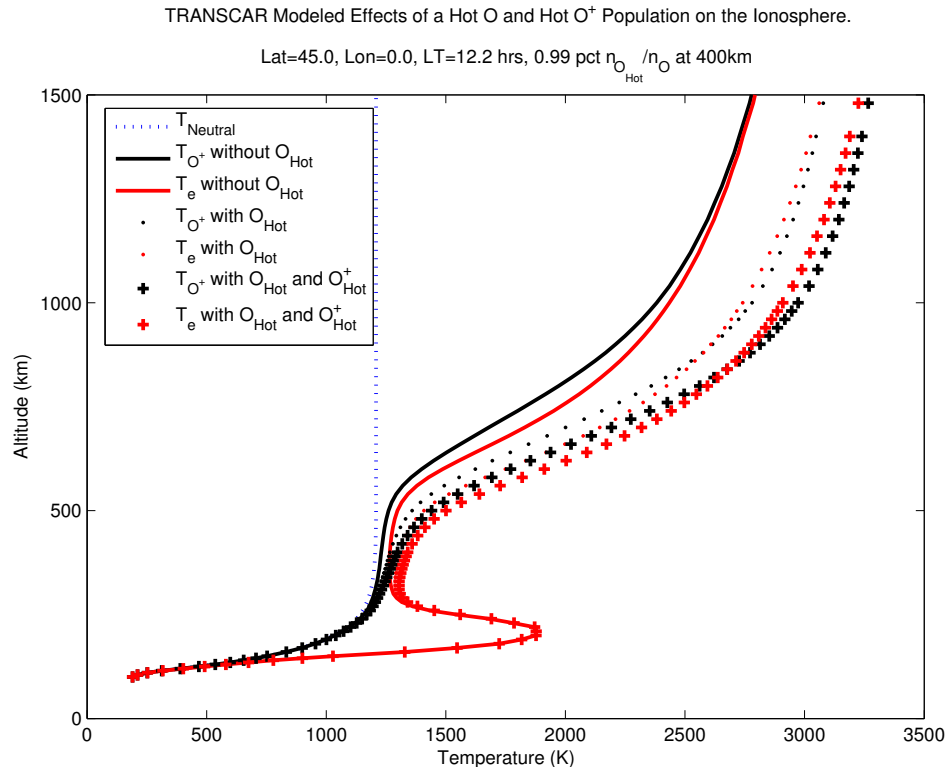


Fig. 3. Comparison of temperatures calculated by TRANSCAR for 3 different simulations: control sim., sim. with hot O, and sim. with hot O and hot O⁺. T_{Neutral} is the cold neutral temperature, T_{O^+} is the O⁺ temperature, and T_e is the electron temperature.

where

$$H(z) = \frac{k_b T}{mg(z)}. \quad (19)$$

The reference density, $n(z_0)$ is taken to be 1% of the cold O density at $z_0=400$ km:

$$n_{\text{O}_{\text{hot}}}(400 \text{ km}) = 0.01 \cdot n_{\text{O}}(400 \text{ km}) \quad (20)$$

The temperature for hot O is chosen to be 4000 K at all altitudes.

Other neutral species are obtained by TRANSCAR from the MSIS model (Hedin, 1991). The high temperature of hot O gives it a large scale height and causes it to become progressively more important than ambient O at higher altitudes. An example of the neutral atmosphere calculated in TRANSCAR is shown in Fig. 2. Hot O affects the ions via collisions. These collision terms are added into the momentum, energy, and heat flow equations for all ions in TRANSCAR.

When we run TRANSCAR with the hot O in the simulation, the most pronounced effect is on the ion temperature. Figure 3 shows that even the trace amount (1% at 400 km) of hot O included in the simulation has significant effect on the ion temperature, especially at high altitudes. At lower altitudes, hot O is present only in small concentrations relative to the cooler neutral species densities (Fig. 2), so any energy imparted to an ion by a collision with a hot O atom is quickly

lost due to the relatively high collision frequency of the ion with the cooler neutral species. At higher altitudes hot O becomes the most common neutral species, and, thus, has a more significant effect on the ion temperature (Alcayd  et al., 2001). At these altitudes ion collisions with hot O atoms are more frequent than with any other neutral species. Thus, energy imparted to the ions is not lost as quickly via collisions with the cooler neutrals. The result is that, at higher altitudes, the ions are hotter by about ≈ 300 K in the simulation with hot O than they are in the control simulation.

These simulations exhibit the non-monotonic electron temperature profile that is characteristic of solar max. This decrease in electron temperature near the F-region peak is a result of the very high electron density there during solar max. Since the electron temperature is inversely related to density (Rishbeth and Garriot, 1969), this causes the temperature profile to “dip” at altitudes where the electron density is extremely high.

6 Simulation of hot O⁺

In order to self-consistently model hot O⁺, we now alter TRANSCAR to solve its continuity, momentum, energy and heat flow equations. Hot O⁺ is produced from hot O as a result of photoionization and charge exchange chemistry. The

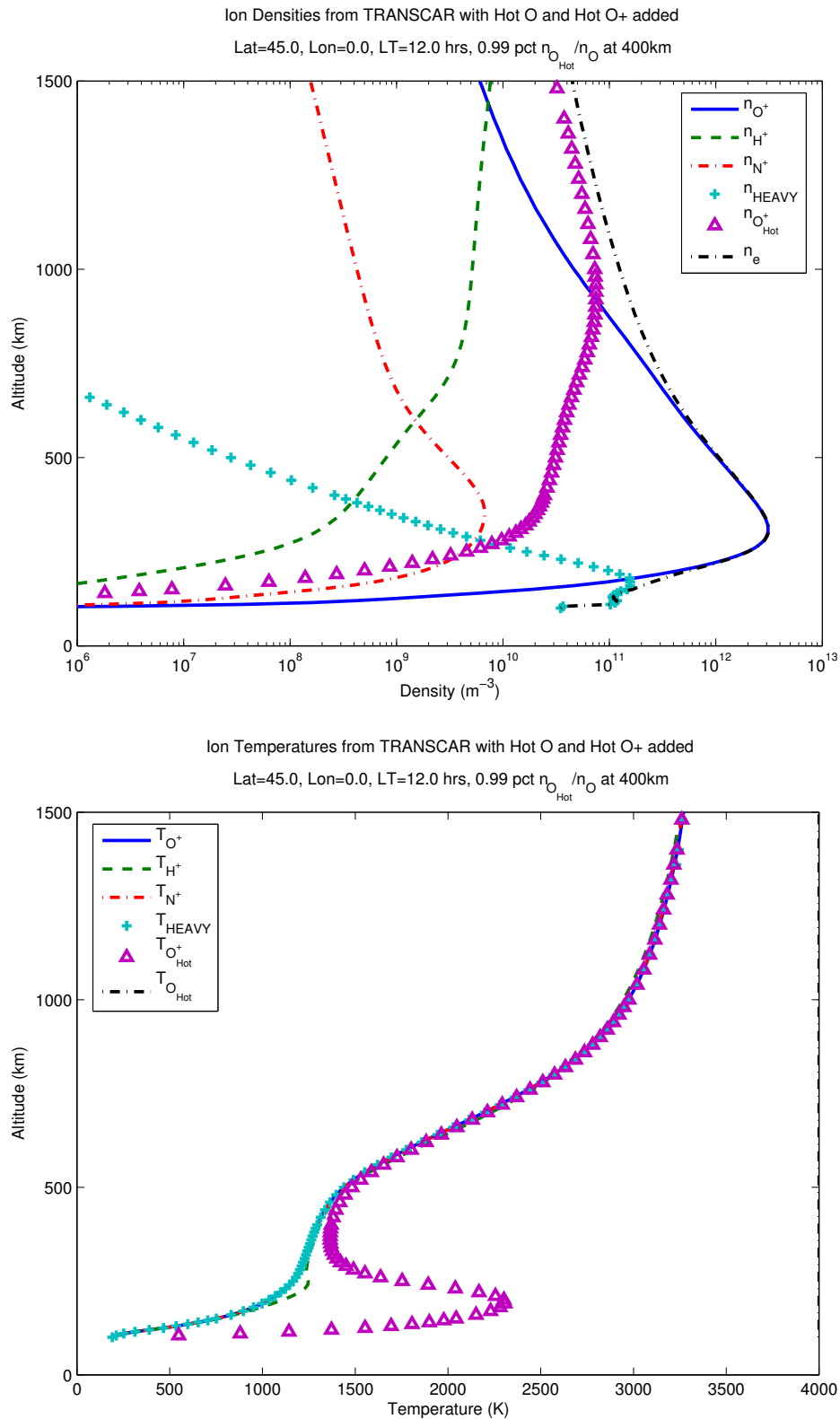


Fig. 4. Ion densities n_s and temperatures T_s as simulated in TRANSCAR. This simulation includes our self-consistently modeled population of hot O^+ .

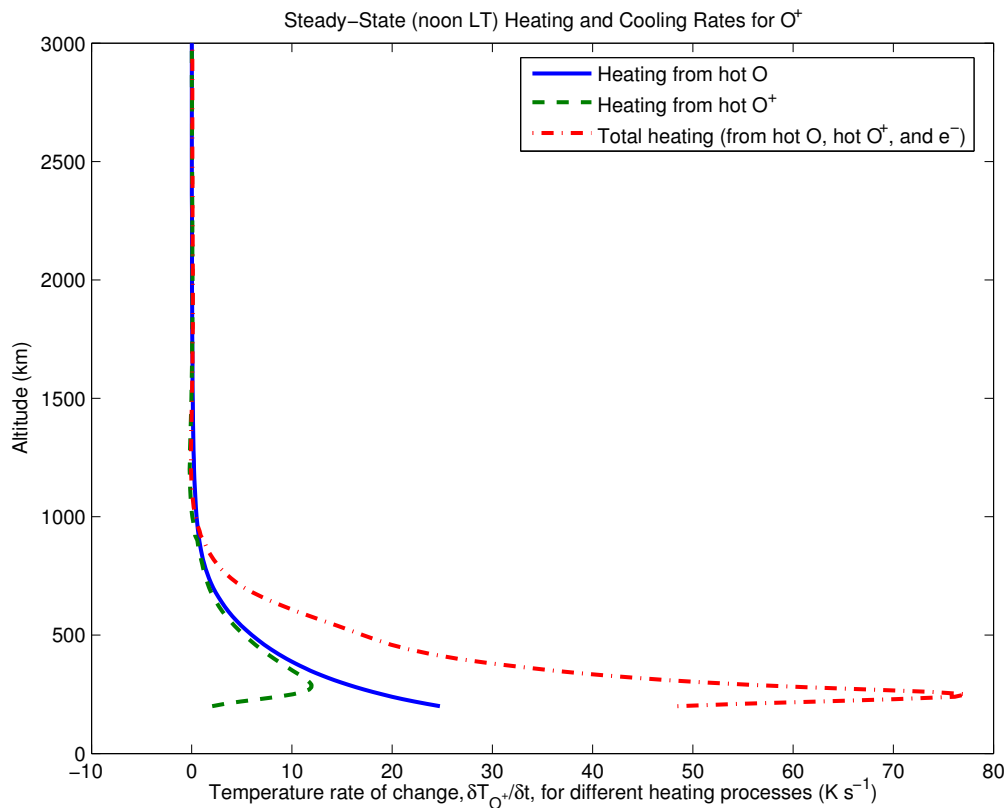


Fig. 5. O^+ noontime heating rates due to collisions with hot O, hot O^+ , and e^- . The total steady-state cooling rate (from collisions with neutral atoms) is equal to the total heating rate shown above.

chemical model that we use to describe hot O^+ is shown in Table 1. Reactions R_1 and R_2 represent sources of hot O^+ and reactions R'_1 – R'_4 represent losses. Our simulations show that charge exchange production reactions represent a much larger portion of the overall production rate for hot O^+ than does photoionization. This is not surprising since the ionized reactants for the charge exchange reactions, O^+ and H^+ , are the dominant ions at the F-region peak and topside altitudes, respectively. Also, the ionization potentials for O and H are similar and allow for very fast charge exchange.

In addition to the production and loss effects of hot O^+ on the continuity equations, hot O^+ affects (and is affected by) other ions through collisions. The terms describing these collisions are now added to the appropriate equations, in much the same manner as were the terms for hot O. The collision cross sections for ion-ion interactions are larger than those of ion-neutral interactions, since the potential for Coulomb interaction (ion-ion) is larger than that for Maxwell molecule interactions (ion-neutral). From these considerations, we predict that hot O^+ likely has a significant effect on the ambient ion temperature due to frequent collisions. However, the collisional heat exchange process is two-way. The ambient ions also have an equally significant heating effect on hot O^+ .

A sample plot of the output from TRANSCAR for the simulation including hot O^+ is shown in Fig. 4. As expected the ambient ion population does have a large effect on the energy dynamics of hot O^+ . In fact, the ambient ions cause the hot O^+ to thermalize to the ambient ion temperature at most altitudes, the exception being around the F-region density peak (see Fig. 4). Here ion-ion collision frequencies are the greatest, but production of hot O^+ is also large. The high production rate results in a net heat input, via the source of Eq. (13), into the population and an elevated temperature at the F-region peak. Hot O^+ forms a layer with a peak density of $n_s(z_{pk}) \approx 7.46 \times 10^{10} \text{ m}^{-3}$ at an altitude of $z_{pk} \approx 940 \text{ km}$. These simulated values are reasonably close to the values predicted in section 2, $n_s(z_{pk}) \approx 5.62 \times 10^{10} \text{ m}^{-3}$ and $z_{pk} \approx 840 \text{ km}$. According to the simulation, hot O^+ becomes the major ion at altitudes of 1000 km–2000 km. However, at these altitudes the temperature of hot O^+ is essentially equal to that of O^+ . Thus, the two species are indistinguishable in this altitude regime.

Hot O^+ does not maintain a temperature above that of the rest of the ion population at most altitudes, instead thermalizing to the ambient ion temperature quickly. This result was predicted earlier using an approximate analytic solution to the temperature equation for hot O^+ . From our simulation

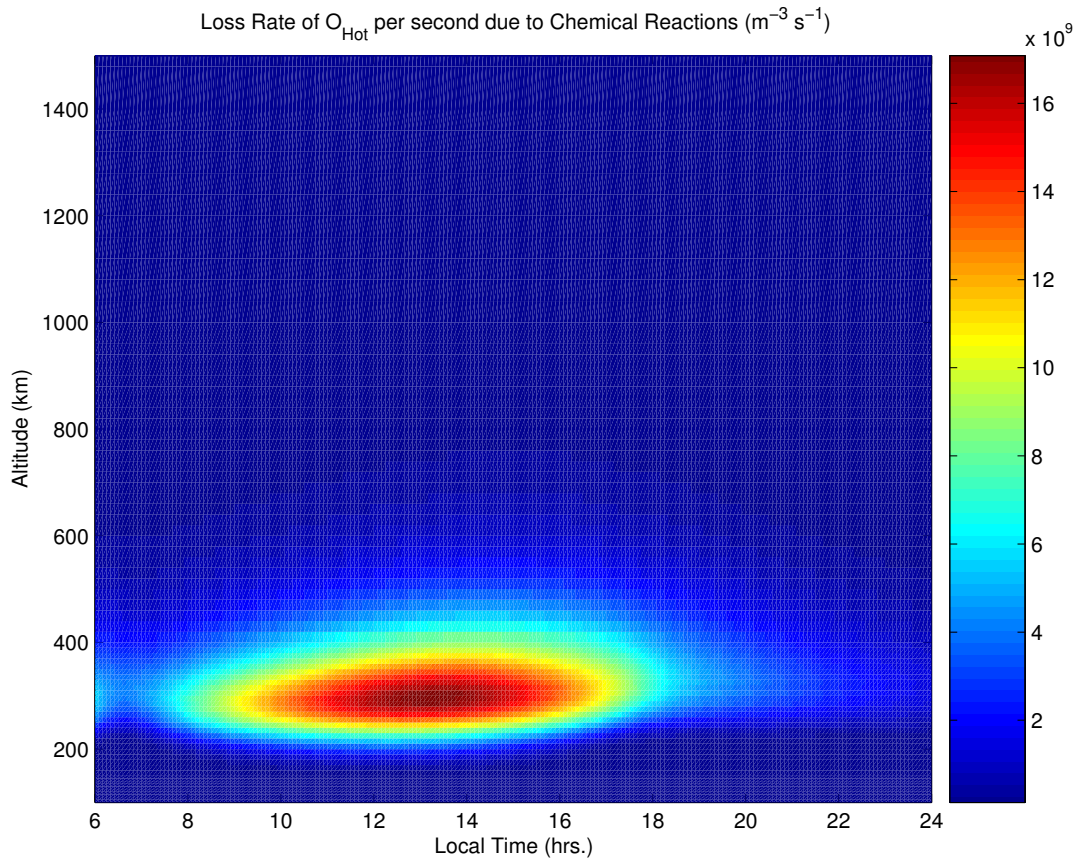


Fig. 6. Loss rate for neutral hot O.

results, we conclude that the ratio P_s/n_s from Eq. (17) is small for hot O^+ at most altitudes. Earlier we calculated the thermalization time constant to be inversely proportional to the weighted sum of the collision frequencies O^+ and H^+ . To see how accurate these calculations are, we have run a simplified hot O^+ simulation that omits the effects of productions, energy transport, and drag on the hot O^+ . Using this simulation, we obtain from the time-dependent temperature output a time constant which may be compared with that estimated analytically from Eq. (10). Figure 1 shows that these two time constants follow the same general trend with altitude. τ ranges from ≈ 0.5 min at lower altitudes to ≈ 2 min at the highest altitudes that we simulate.

Hot O^+ does not thermalize completely near the F-region peak. This is a result of the heat source of Eq. (13). At the F-region peak the hot O^+ density is low due to loss processes involving H, O, O_2 , and N_2 . However, the O^+ density is at its peak so there is still a large hot O^+ production rate from reaction R_2 of Table 1. This results in a significant heat source for the hot O^+ population and alters its equilibrium temperature to be greater than that of the ambient ions.

The introduction of hot O^+ into TRANSCAR has a considerable effect on the rest of the simulated ionosphere.

Specifically, hot O^+ is a heat source for the ambient ions. Figure 3 shows that hot O^+ has the effect of increasing the ambient ion temperature, *in addition* to the increase imposed by the neutral hot O. At higher altitudes the presence of hot O^+ has the effect of raising the ambient ion temperature another ≈ 150 K above the temperature of the simulation with neutral hot O. This is a direct result of the thermalization of hot O^+ . Hot O^+ collides with and imparts its energy to the ambient ion population. Consequently, hot O^+ thermalizes to the ambient ion temperature, but, in the process, causes the ambient temperature to increase. A plot of the heat input to the O^+ population due to collisions with hot O and hot O^+ is shown in Fig. 5. This figure shows that hot O and hot O^+ are comparably important heat sources for the ambient ions. The simulation with hot O^+ also shows small but noticeable effects on the densities of O^+ and H^+ (due to reactions R_1 , R'_1 , R_2 , and R'_2 in Table 1, and changes in scale height) when compared to the control simulation (the simulation without hot O).

Hot O^+ represents a sink for neutral hot O through chemical reactions R_1 and R_2 in Table 1. We can use our simulation to evaluate the loss rate of hot O due to the chemical production of hot O^+ . The results of this evaluation are

Table 2. Hot O⁺ cooling reactions.

(R _{th,1})	$O_{\text{hot}}^+ + O^+ \xrightarrow{k_{th,1}} O^+ + O^+$
(R _{th,2})	$O_{\text{hot}}^+ + H^+ \xrightarrow{k_{th,2}} H^+ + O^+$

shown in Fig. 6. The percentage loss of hot O due to production of hot O⁺ has a maximum at the F-region peak of $\approx 3.5\%$ of the total hot O population over a period of 18 hrs. Comparison of Fig. 6 with the production rates for hot O calculated in Richards et al. (1994) and Hickey et al. (1995) reveals that the loss rate is comparable to the hot O production rate of from the dominant production reaction considered, $N_2(\nu=1)+O \rightarrow N_2(\nu=0)+O_{\text{hot}}$.

7 Implications for the overall O⁺ population

Since simulations show that hot O⁺ is nearly indistinguishable from ambient O⁺, we have combined the moments of the separate species back into one collective O⁺ population. The distribution function for the collective O⁺ species is given by:

$$f = f_{s_1} + f_{s_2} \quad (21)$$

for $s_1=O^+$ and $s_2=O_{\text{hot}}^+$. The moments of the O⁺ distribution function can be calculated in terms of the moments of the separate species by using this distribution function:

$$\begin{aligned} n &= \int_{-\infty}^{\infty} f d^3v \\ &= \int_{-\infty}^{\infty} (f_{s_1} + f_{s_2}) d^3v \\ &= n_{s_1} + n_{s_2}. \end{aligned} \quad (22)$$

Likewise,

$$\begin{aligned} \mathbf{u} &= \frac{1}{n} \int_{-\infty}^{\infty} \mathbf{v} (f_{s_1} + f_{s_2}) d^3v \\ &= \frac{1}{n_{s_1} + n_{s_2}} \left(\int_{-\infty}^{\infty} \mathbf{v} f_{s_1} d^3v + \int_{-\infty}^{\infty} \mathbf{v} f_{s_2} d^3v \right) \\ &= \frac{n_{s_1} \mathbf{u}_{s_1} + n_{s_2} \mathbf{u}_{s_2}}{n_{s_1} + n_{s_2}}. \end{aligned} \quad (23)$$

The heat flow is more complicated but can be found in the same manner.

$$\mathbf{q} = \frac{1}{2} m \int_{-\infty}^{\infty} (\mathbf{v} - \mathbf{u})^2 (\mathbf{v} - \mathbf{u}) (f_{s_1} + f_{s_2}) d^3v \quad (24)$$

Analysis of this expression simplifies if we introduce the following variables:

$$\Delta \mathbf{u}_{s_1} = \mathbf{u}_{s_1} - \mathbf{u} = \frac{n_{s_2}}{n} (\mathbf{u}_{s_1} - \mathbf{u}_{s_2})$$

$$\Delta \mathbf{u}_{s_2} = \mathbf{u}_{s_2} - \mathbf{u} = \frac{n_{s_1}}{n} (\mathbf{u}_{s_2} - \mathbf{u}_{s_1})$$

Substituting these variables for \mathbf{u} , the heat flow equation becomes:

$$\begin{aligned} \mathbf{q} &= \frac{1}{2} m \int_{-\infty}^{\infty} \left[(\mathbf{v} - \mathbf{u}_{s_1} + \Delta \mathbf{u}_{s_1})^2 \right. \\ &\quad \left. (\mathbf{v} - \mathbf{u}_{s_1} + \Delta \mathbf{u}_{s_1}) f_{s_1} \right] d^3v \\ &\quad + \frac{1}{2} m \int_{-\infty}^{\infty} \left[(\mathbf{v} - \mathbf{u}_{s_2} + \Delta \mathbf{u}_{s_2})^2 \right. \\ &\quad \left. (\mathbf{v} - \mathbf{u}_{s_2} + \Delta \mathbf{u}_{s_2}) f_{s_2} \right] d^3v \end{aligned}$$

If the velocity product terms are expanded, this equation becomes (after much algebra):

$$\begin{aligned} \mathbf{q} &= \mathbf{q}_{s_1} + m \int_{-\infty}^{\infty} [(\mathbf{v} - \mathbf{u}_{s_1}) \Delta \mathbf{u}_{s_1}] (\mathbf{v} - \mathbf{u}_{s_1}) f_{s_1} d^3v \\ &\quad + \left(\frac{1}{2} m \int_{-\infty}^{\infty} (\mathbf{v} - \mathbf{u}_{s_1})^2 f_{s_1} d^3v \right. \\ &\quad \left. + \frac{1}{2} m \Delta \mathbf{u}_{s_1}^2 \int_{-\infty}^{\infty} f_{s_1} d^3v \right) \Delta \mathbf{u}_{s_1} \\ &\quad + \mathbf{q}_{s_2} + m \int_{-\infty}^{\infty} [(\mathbf{v} - \mathbf{u}_{s_2}) \Delta \mathbf{u}_{s_2}] (\mathbf{v} - \mathbf{u}_{s_2}) f_{s_2} d^3v \\ &\quad + \left(\frac{1}{2} m \int_{-\infty}^{\infty} (\mathbf{v} - \mathbf{u}_{s_2})^2 f_{s_2} d^3v \right. \\ &\quad \left. + \frac{1}{2} m \Delta \mathbf{u}_{s_2}^2 \int_{-\infty}^{\infty} f_{s_2} d^3v \right) \Delta \mathbf{u}_{s_2} \end{aligned} \quad (25)$$

This expression can be simplified to an equivalent expression in terms of the moments of the two distributions:

$$\begin{aligned} \mathbf{q} &= \mathbf{q}_{s_1} + n_{s_1} k_b T_{s_1} \Delta \mathbf{u}_{s_1} \\ &\quad + \left(\frac{3}{2} n_{s_1} k_b T_{s_1} \right. \\ &\quad \left. + \frac{1}{2} m \Delta \mathbf{u}_{s_1}^2 \right) \Delta \mathbf{u}_{s_1} \\ &\quad + \mathbf{q}_{s_2} + n_{s_2} k_b T_{s_2} \Delta \mathbf{u}_{s_2} \\ &\quad + \left(\frac{3}{2} n_{s_2} k_b T_{s_2} \right. \\ &\quad \left. + \frac{1}{2} m \Delta \mathbf{u}_{s_2}^2 \right) \Delta \mathbf{u}_{s_2} \end{aligned} \quad (26)$$

If like terms are gathered, then the equation for heat flow becomes:

$$\begin{aligned} \mathbf{q} &= \mathbf{q}_{s_1} + \mathbf{q}_{s_2} + \frac{n_{s_1} n_{s_2}}{n_{s_1} + n_{s_2}} \left(\frac{5}{2} k_b (T_{s_1} - T_{s_2}) \right. \\ &\quad \left. + \frac{1}{2} m \frac{n_{s_2} - n_{s_1}}{n_{s_1} + n_{s_2}} (\mathbf{u}_{s_1} - \mathbf{u}_{s_2})^2 \right) (\mathbf{u}_{s_1} - \mathbf{u}_{s_2}) \end{aligned} \quad (27)$$

If there is a differential drift velocity, $\mathbf{u}_{s_1} - \mathbf{u}_{s_2}$, between the two species of O⁺, then the heat flow for the collective O⁺

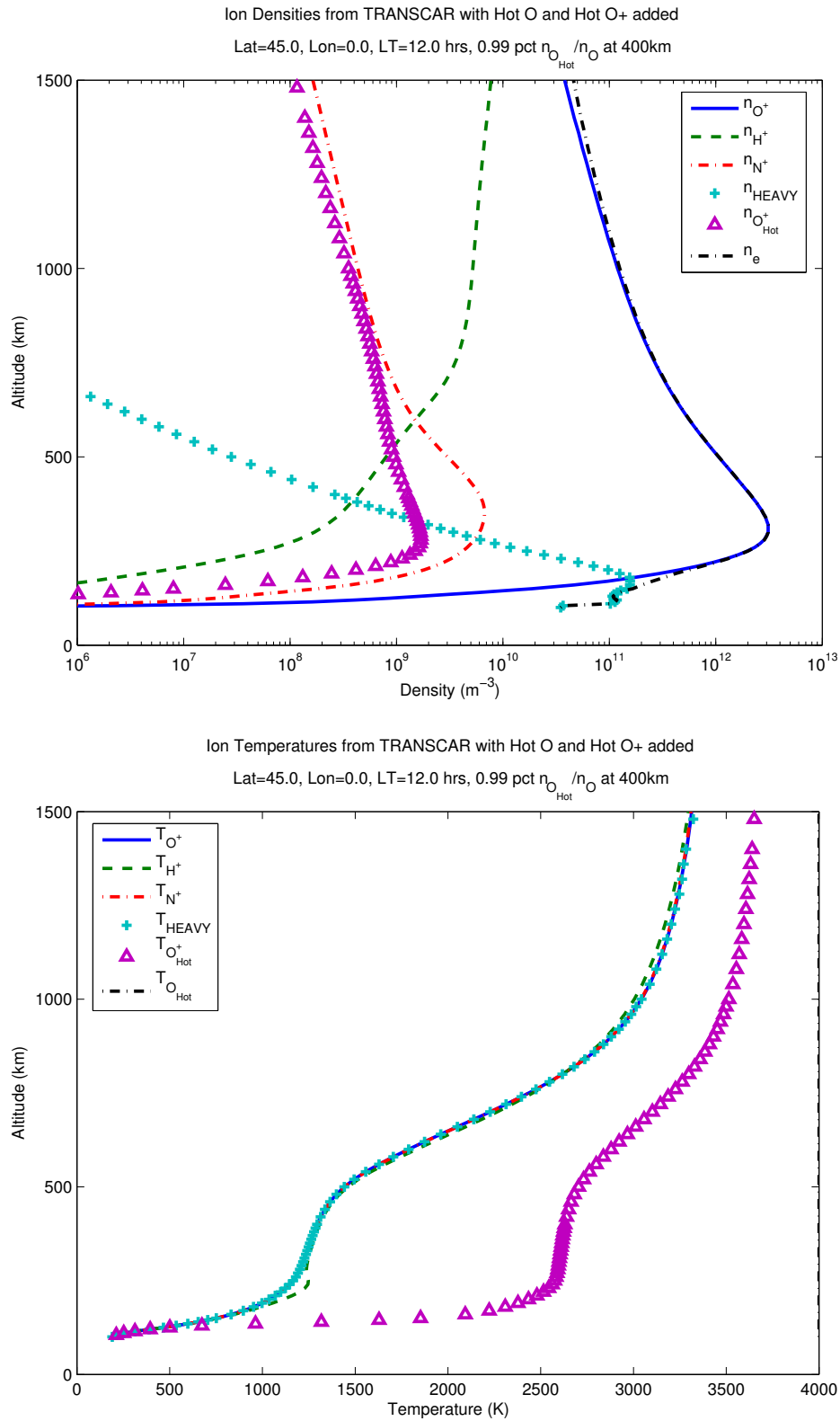


Fig. 7. Ion densities n_s and temperatures T_s as simulated in TRANSCAR. This simulation includes our self-consistently modeled population of hot O^+ , with thermalization losses included.

ion will contain a significant contribution from the differential drift. The simulations show that while the hot O^+ particles may not constitute a separate species, they may manifest themselves through an enhanced heat flow in the overall O^+ population, via the differential drift velocity. However, hot O^+ and ambient O^+ do not maintain enough drift velocity difference (even during sunrise and sunset) to cause the overall heat flow to deviate substantially from the sum of the individual heat flows.

8 Thermalization as a loss process

To this point the hot O^+ has been treated as a completely separate species from O^+ . However, when hot O^+ thermalizes to the ambient O^+ temperature there is no feature that differentiates the hot O^+ from the ambient O^+ . The thermalization can be considered a loss process for the hot O^+ . If hot O^+ is modeled this way, then the density will be lower than in our simulations and this will affect the equilibrium temperature of the hot O^+ , since the ratio P_s/n_s will be larger (Eq. 17). We present here a simulation of this alternative model of hot O^+ .

We model the effects of thermalization loss by adding in two cooling reactions, $R_{th,1}$ and $R_{th,2}$ of Table 2.

The total loss frequency for these reactions, β_{th} , is taken to be the inverse time constant for thermalization that was derived in section 3.

$$\beta_{th} = k_{th,1}n_{O^+} + k_{th,2}n_{H^+} = \frac{1}{\tau} = \nu' \quad (28)$$

ν' is from Eq. (10).

To fully model the thermalization reactions of Table 2, we must also include the energy input into the O^+ and H^+ populations due to these reactions. The energy input has the form of Eq. (13):

$$\left(\frac{\delta T_s}{\delta t}\right)^* = \frac{P_s (T_{O^+_{hot}} - T_s)}{n_s} \quad (29)$$

For this case, $s=O^+, H^+$. Figure 7 shows the TRANSCAR results for the ionosphere with hot O^+ thermalization losses included. Figure 7 shows that the new thermalization loss reactions cause the hot O^+ density to be much lower. As a consequence the heat source of Eq. (13), which is inversely proportional to density, is large enough to keep the hot O^+ at a significantly higher temperature than the ambient ions (Fig. 7). However, the hot O^+ would still not be detectable, since it has such a low density.

The heating effects of hot O^+ on the ambient O^+ now include two components: collisional heating, $\delta T_s/\delta t$, and a production heating $(\delta T_s/\delta t)^*$. Our simulations show that if these two components are added together, they equal the hot O^+ heating rate computed from our original model of hot O^+ , Fig. 5.

9 Conclusions

Our findings indicate that hot O^+ does not maintain a temperature above that of the ambient ions, but is an important heat source for the ambient ions.

We have made approximate calculations describing the behavior of hot O^+ . Also we have made additions to an existing simulation of the ionosphere (TRANSCAR) in order to investigate the possible effects of a hypothesized neutral hot O population and a self-consistently modeled hot O^+ population. Since it has a considerably higher temperature than the ambient ions, neutral hot O serves as a significant heat source to the ionosphere at all altitudes (Fig. 3). However, hot O^+ cannot maintain an elevated temperature at most altitudes due to thermalization by the other ions (Fig. 4). Through this process of thermalization, hot O^+ represents a heat source (in addition to the hot O heat source) for the ambient ions (Fig. 5). Figure 3 shows that the inclusion of hot O^+ causes the ambient ion temperature to be higher than in the control simulation (no hot O, no hot O^+) and the simulation with only hot O. From Figs. 3 and 5 it can be seen that the combined effect of the hot O and hot O^+ on the energy dynamics of the ionosphere is considerable.

Figure 4, which is representative of the noontime, steady-state ionosphere, shows that hot O^+ is the dominant ion at 1000 km–2000 km altitude. The temperature of hot O^+ is approximately equal to the ambient ion temperature (Fig. 4) at these altitudes, so that there is really no distinction between hot O^+ and O^+ . The ionization of hot O and the subsequent thermalization of hot O^+ appears to be an efficient heating process in the ionosphere.

We have also considered an alternative way to model hot O^+ that includes the thermalization process as a loss process in the continuity equation. This alternate model gives a significantly different density and temperature profile. However, the heating effects of hot O^+ on the ambient ions remains the same as before. Since detecting hot O^+ does not appear to be feasible, the heating effects, which are the same under both models, are the most important aspect of hot O^+ .

Acknowledgements. M. D. Zettergren would like to thank the fine folks of CESR in Toulouse, France for hosting him while he worked on this research, in particular: J. Fontanari, V. Boqueho, and C. Peymirat. M. D. Zettergren and W. L. Oliver were supported for this work under US /NSF grant ATM-0327625.

Topical Editor M. Pinnock thanks P. Richards and J. Meriwether for their help in evaluating this paper.

References

- Alcaydé, D., Blelly, P.-L., Kofman, W., Litvin, A., and Oliver, W. L.: Effects of hot oxygen in the ionosphere: TRANSCAR simulations, *Ann. Geophys.*, 19, 257–261, 2001.
- Blelly, P.-L., Liliensten, J., Robineau, A., Fontanari, J., and Alcaydé, D.: Calibration of a numerical ionospheric model with EISCAT observations, *Ann. Geophys.*, 14, 1375–1390, 1996a.

- Blelly, P.-L., Robineau, A., Liliensten, J., and Lummerzheim, D.: 8-moment fluid models of the terrestrial high latitude ionosphere between 100 and 3000 km, in: Solar Terrestrial Energy Program (STEP): Handbook of Ionospheric Models, edited by: Schunk, R. W., 53–72, 1996b.
- Cotton, D. M., Gladstone, G. R., and Chakrabarti, S.: Sounding rocket observation of a hot oxygen geocorona, *J. Geophys. Res.*, 98, 21 651–21 657, 1993.
- Diloy, P.-Y., Robineau, A., Liliensten, J., and Lummerzheim, D.: A numerical model of the ionosphere, including the E-region above EISCAT, *Ann. Geophys.*, 14, 191–200, 1996.
- Hedin, A. E.: Hot oxygen geocorona as inferred from neutral exospheric models and mass spectrometer measurements, *J. Geophys. Res.*, 94, 5523–5529, 1989.
- Hedin, A. E.: Extension of the MSIS thermospheric model into the middle and lower atmosphere, *J. Geophys. Res.*, 96, 1159–1172, 1991.
- Hernandez, G.: The signature profiles of $O(^1S)$ in the airglow, *Planet. Space Sci.*, 19, 467–476, 1971.
- Hickey, M. P., Richards, P. G., and Torr, D. G.: New sources for the hot oxygen geocorona: Solar cycle, seasonal, latitudinal, and diurnal variations, *J. Geophys. Res.*, 100, 17 377–17 388, 1995.
- Keating, G. M., Leary, J. C., Green, B. D., Uy, O. M., Benson, R. C., Erlandson, R. E., Philips, T. E., Lesho, J. C., and Boies, M. T.: Neutral and ion drag effects near the exobase: MSX satellite measurements of He and O^+ , *Adv. Aeron. Sci.*, 97, 549–556, 1997.
- Livtin, A. and Oliver, W. L.: Hot O and nighttime ionospheric temperatures, *Geophys. Res. Lett.*, 27, 2821–2824, 2000.
- Oliver, W. L.: Hot oxygen and the ion energy budget, *J. Geophys. Res.*, 102, 2503–2511, 1997.
- Oliver, W. L. and Glotfelty, K.: O^+ -O collision cross section and long-term F region O density variations deduced from the ionospheric energy budget, *J. Geophys. Res.*, 101, 21 769–21 784, 1996.
- Oliver, W. L. and Schoendorf, J.: Variations of hot O in the thermosphere, *Geophys. Res. Lett.*, 26, 2829–2832, 1999.
- Richards, P. G., Hickey, M. P., and Torr, D. G.: New sources for the hot oxygen geocorona, *Geophys. Res. Lett.*, 21, 657–660, 1994.
- Rishbeth, H., and Garriot, O. K.: *Introduction to Ionospheric Physics*, Academic Press, 1969.
- Rohrbaugh, R. P. and Nisbet, J. S.: Effect of energetic oxygen atoms of neutral density models, *J. Geophys. Res.*, 78, 6768–6772, 1973.
- Schoendorf, J., Young, L. A., and Oliver, W. L.: Hot oxygen profiles for incoherent scatter radar analysis of ion energy balance, *J. Geophys. Res.*, 105, 12 823–12 832, 2000.
- Shematovich, V. I., Bisikalo, D. V., and Gérard, J. C.: A kinetic model of the formation of the hot oxygen geocorona 1. Quiet geomagnetic conditions, *J. Geophys. Res.*, 99, 23 217–23 228, 1994.
- Stancil, P. C., Schultz, D. R., Kimura, M., Gu, J.-P., Hirsch, G., and Buenker, R. J.: Charge transfer in collisions of O^+ with H and H^+ with O, *Astron. Astrophys. Suppl. Ser.*, 140, 225–234, 1999.
- Yee, J. H., Meriwether, J. W., and Hayes, P. B.: Detection of a corona of fast oxygen atoms during solar maximum, *J. Geophys. Res.*, 85, 3396–3400, 1980.